eprints@whiterose.ac.uk
https://eprints.whiterose.ac.uk/

Photon Statistics of Filtered Resonance Fluorescence

Catherine L. Phillips[1], Alistair J. Brash[1,*], Dara P. S. McCutcheon,[2] Jake Iles-Smith,[1,3,4] Edmund Clarke,[5]
Benjamin Royall,[1] Maurice S. Skolnick,[1] A. Mark Fox[1], and Ahsan Nazir[3,†]

[1]*Department of Physics and Astronomy, University of Sheffield, Sheffield S3 7RH, United Kingdom*
[2]*Quantum Engineering Technology Labs, H. H. Wills Physics Laboratory and Department of Electrical and Electronic Engineering,
University of Bristol, Bristol BS8 1FD, United Kingdom*
[3]*Department of Physics and Astronomy, The University of Manchester, Oxford Road, Manchester M13 9PL, United Kingdom*
[4]*Department of Electrical and Electronic Engineering, The University of Manchester,
Sackville Street Building, Manchester M1 3BB, United Kingdom*
[5]*EPSRC National Epitaxy Facility, Department of Electronic and Electrical Engineering, University of Sheffield,
Sheffield S1 3JD, United Kingdom*

Spectral filtering of resonance fluorescence is widely employed to improve single photon purity and indistinguishability by removing unwanted backgrounds. For filter bandwidths approaching the emitter linewidth, complex behavior is predicted due to preferential transmission of components with differing photon statistics. We probe this regime using a Purcell-enhanced quantum dot in both weak and strong excitation limits, finding excellent agreement with an extended sensor theory model. By changing only the filter width, the photon statistics can be transformed between antibunched, bunched, or Poissonian. Our results verify that strong antibunching and a subnatural linewidth cannot simultaneously be observed, providing new insight into the nature of coherent scattering.

Resonance fluorescence (RF) of two-level emitters (TLEs) is integral to numerous important proposals for optical quantum technologies such as single photon sources [1–3], spin-photon entanglement [4,5] and entanglement of remote spins [6,7]. The emitted spectrum is well suited to these applications, exhibiting strong single-photon anti-bunching and, under appropriate excitation conditions, a dominant coherently scattered component with a subnatural linewidth inherited from the laser coherence. Indeed, an ideal TLE in the limit of vanishing driving strength would exhibit both perfect antibunching and a coherent fraction approaching unity. Experimentally, studies have observed both strong antibunching and high coherent fractions in separate measurements performed under identical conditions [8–10]. It is thus perhaps intuitive to assume that this coherent component must itself be antibunched. However this is not the case; by exploiting spectral filtering we demonstrate that, in accordance with theoretical predictions [11,12], antibunching requires interference between coherent and incoherent scattering and consequently cannot be observed simultaneously with a subnatural linewidth.

In experimental quantum optics, spectral filtering around the zero phonon line (ZPL) of a TLE is widely employed to remove unwanted backgrounds from the driving laser [1,3], other transitions [13], or phonon sidebands [13–15], improving the measured single photon purity and indistinguishability. Considering only indistinguishability, reducing the filter bandwidth always gives an improvement (at the cost of

efficiency) as more background is removed [16]. However, as the filter bandwidth approaches the natural linewidth (γ) of the ZPL, theory predicts strongly modified photon statistics in both weak (coherent scattering) [12,17] and strong (Mollow triplet) [18] driving regimes, an effect generally overlooked in experiments to date. Here, we experimentally verify these predictions, combining our results with a theoretical model to develop a thorough understanding of the complex photon statistics associated with spectrally filtered resonance fluorescence. These concepts are equally applicable to the broad assortment of atomic and atomlike TLEs used in current quantum optics research.

The sample is studied in a liquid helium bath cryostat at 4.2 K and incorporates a self-assembled InGaAs quantum dot (QD) into an H1 photonic crystal cavity with coupled W1 waveguides [Fig. 1(a)]. Resonant continuous wave (CW) laser excitation and collection of emission is made from directly above the cavity whilst laser backscattering is rejected using a cross-polarization technique. A p-i-n diode structure allows the QD neutral exciton to be electrically tuned. At the cavity resonance, a maximum Purcell factor of 43 shortens the QD's radiative lifetime (T_1) to 22.7 ps and results in lifetime-limited coherence [3]. Here, the QD is slightly detuned from the cavity, giving a Purcell factor of ~30 and a broad natural linewidth (γ) of 20 μeV. This large γ enables exploration of filter bandwidths (Γ) $\leq \gamma$ using a combination of diffraction grating and etalon filters (details in the Supplemental Material [19]).
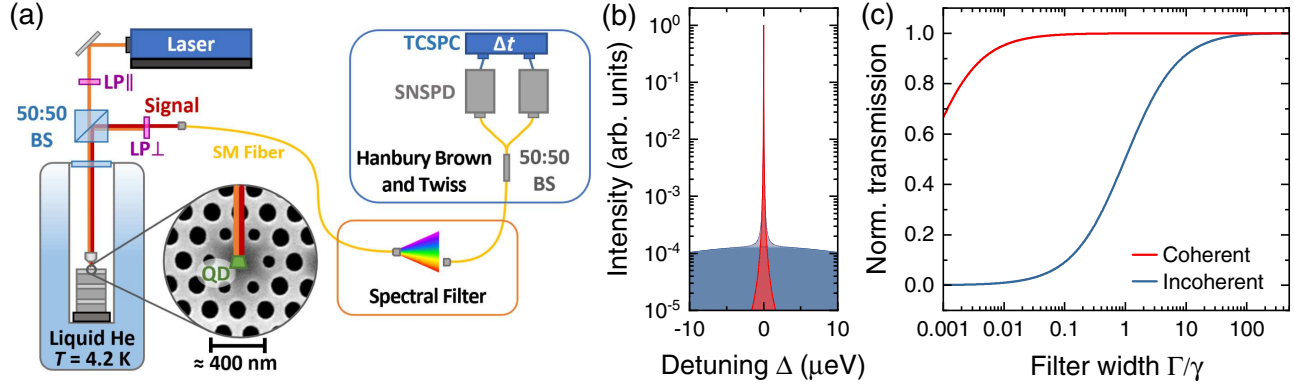
FIG. 1. (a) Experimental setup: LP—linear polarizer, BS—beam splitter, SM—single mode fiber, SNSPD—superconducting nanowire single photon detectors, TCSPC—time correlated single photon counter. (b) The calculated QD emission spectra (purple) under weak excitation comprises incoherent (blue) emission with 20 μeV linewidth from spontaneous and stimulated emission and a narrow coherent (red) component that inherits the 10 neV linewidth of the CW laser; both components are modeled with a Lorentzian line shape. (c) Transmission coefficients of the coherent (red) and incoherent (blue) parts of the QD spectra through an ideal Lorentzian filter of width Γ. Changing Γ strongly modifies the ratio of the two components.

For resonant CW excitation and a lifetime-limited emitter coherence time ($T_2 = 2T_1$), the weak excitation limit is defined as $\Omega_R^2 < (\gamma^2/2)$ where Ω_R is the Rabi frequency and $\gamma = 1/T_1$ [28]. This is often termed the resonant Rayleigh scattering (RRS) or Heitler regime [8,29,30]. The RF spectrum in this regime includes contributions from both coherent RRS and an incoherent part originating from spontaneous and stimulated emission [9,31]. For coherent scattering, excitation and emission become a single coherent event where the elastically scattered photons inherit the laser coherence, leading to a *subnatural* linewidth [3,8,10,30–32] that illustrates the long coherence times possible in this regime. Meanwhile, the *natural linewidth* of the incoherent component is given by $\gamma = 1/T_1$. Theory suggests that for weak excitation, interference between these different components is the origin of the observed photon antibunching [12]. Owing to the discrepancy in linewidth between coherent and incoherent components, filtering with width $\Gamma < \gamma$ inevitably alters the ratio of the different components, modulating the interference between them and thus the observed photon statistics.

To explore this, Hanbury Brown and Twiss (HBT) measurements [33] of the second-order correlation function [$g^{(2)}(t)$] were performed in the weak CW driving regime. A value of $g^{(2)}(0) < 1$ corresponds to antibunched emission whilst a value of $g^{(2)}(0) = 1$ corresponds to the Poissonian statistics of a coherent source such as a laser. The QD is resonantly excited at laser energy $\hbar\omega_L$, inducing a Rabi frequency $\Omega_R = 0.5\ \gamma$. The emission is collected in cross-polarization with signal-to-background ratio > 100∶1 [19]. It then passes through a filter centered on the ZPL (details in Ref. [19]) before being split by a 50∶50 fiber beam splitter to a pair of superconducting nanowire single photon detectors (SNSPD) connected to a time-correlated single photon counting module (TCSPC), shown

schematically in Fig. 1(a). The SNSPDs have a Gaussian instrument response function (IRF) with 37.5 ± 0.1 ps full-width half-maximum.

Figure 1(b) illustrates the theoretical total spectrum (purple) of the QD under these conditions (see Ref. [19] for corresponding experimental spectrum), comprising an incoherent peak with $\gamma = 20\ \mu$eV (blue) and a coherent peak with a linewidth of ~ 10 neV inherited from the laser (red). The area of the coherent peak relative to the total spectrum is the coherent fraction $\mathcal{F}_{CS}$ [28]:

$$\mathcal{F}_{CS} = \frac{1}{1 + 2\Omega_R^2/\gamma^2}, \qquad (1)$$

which gives $\mathcal{F}_{CS} = 2/3$ for $\Omega_R = 0.5\ \gamma$. The transmission coefficients of the coherent and incoherent parts through an ideal Lorentzian filter with bandwidth Γ are plotted in Fig. 1(c). As Γ is reduced, the transmission of the incoherent component decreases much faster than the coherent component owing to the large (2000×) linewidth difference. Spectral filtering can thus manipulate this ratio up to a limiting case where narrow filtering removes the incoherent component almost entirely.

The variation of $g^{(2)}(0)$ with Γ is shown in Fig. 2(a) for $\Omega_R = 0.5\ \gamma$. As expected for an unfiltered ideal TLE, strong antibunching is observed where the filter bandwidth exceeds the natural linewidth ($\Gamma > \gamma$). At $\Gamma = 150\ \gamma$, $g^{(2)}(0) = 0.09 \pm 0.01$ limited only by the detector IRF (= 1.14 γ^{-1}). However, as the filter bandwidth becomes $\ll \gamma$, the antibunching is lost and $g^{(2)}(0)$ tends towards 1. The experiment agrees well with theoretical predictions [black lines in Fig. 2(a)] derived using the sensor formalism [19–21] with (solid line) or without (dashed line) convolution with the detector IRF.
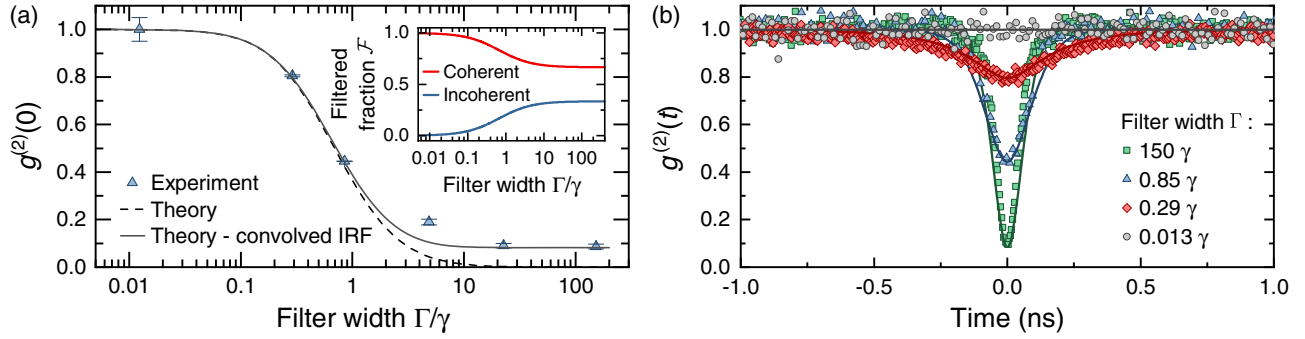
FIG. 2. Filtered photon statistics under weak ($\Omega_R = 0.5\ \gamma$) driving: (a) $g^{(2)}(0)$ measurements (blue triangles) of the exciton emission through different filter bandwidths (Γ), lines show the sensor theory prediction with (solid) and without (dashed) convolution with the detector IRF. Inset: Calculated fraction ($\mathcal{F}$) of the filtered spectrum originating from coherent (red) or incoherent (blue) scattering. (b) Full $g^{(2)}(t)$ measurements from the same dataset exhibit both time broadening and a reduced antibunching dip at narrower filter bandwidths. The solid lines are a sensor theory calculation incorporating the detector IRF.

The sensor theory is equivalent to the calculation of the correlation function from the RF electric field operators, with the sensor damping rates playing the role of the filter width. As previous works have shown [11], the lowest order relevant term in the field contains a coherent and incoherent scattering contribution. These contributions destructively interfere to give zero when no filters are present, and this interference is partially or completely removed when filters are introduced. It is interesting to note that, when moving from $\Gamma = 150\ \gamma$ to $\Gamma = 23\ \gamma$, nearly the entire phonon sideband [25,26,34] is removed with no appreciable change in $g^{(2)}(0)$. The nature of these measurements mean that electron-phonon interaction processes such as excitation-induced dephasing [27] and phonon sideband emission [25,26,34] have negligible impact on $g^{(2)}(t)$. Discussions of the sensor formalism, its extension to include laser background (see below) and phonon effects are given in the Supplemental Material [19].

From Figs. 1(c) and 2(a) we see that the loss of antibunching occurs in the regime ($0.1\ \gamma \lesssim \Gamma \lesssim 10\ \gamma$) where the filter removes almost the entire incoherent component. Indeed, the inset to Fig 2 shows that in this region, the filtered coherent fraction approaches unity. This demonstrates that without both coherent and incoherent contributions, strong antibunching cannot be observed, indicating that the antibunching originates from interference between these components [11,12]. We note that if it were possible to similarly remove only the coherent component, bunched statistics would be expected [11].

Figure 2(b) shows some of the individual $g^{(2)}(t)$ measurements from which Fig. 2(a) is derived. As the filter bandwidth narrows, the central dip in $g^{(2)}(t)$ broadens in width. This can be interpreted according to the uncertainty relation $\Delta E \Delta t > (\hbar/2)$, which implies that a narrower filter (ΔE) inevitably increases the associated timing uncertainty of the photon. Considering that filtering with bandwidth Γ is equivalent to a projective measurement of a photon linewidth $< \Gamma$ [11,12], this illustrates that it is

impossible to simultaneously observe both a subnatural linewidth and strong antibunching from a TLE.

Looking now at the strong driving regime defined as $\Omega_R \gg (1/T_2)$, Fig. 3 shows the resulting ac Stark effect transformation of the "bare" states of the TLE into "dressed" states split by the Rabi energy ($\hbar\Omega_R$). This splitting gives four possible transitions between upper and lower manifolds; as two of the transitions are degenerate, the result is the purple Mollow triplet spectrum shown in Fig. 3 for $\Omega_R = 2\gamma$. The central (Rayleigh) peak is flanked by two side (Mollow) peaks. The width of the individual peaks is governed by γ [35,36]. In addition to these incoherent peaks, a contribution from coherent scattering remains (red). As Ω_R increases, the Mollow splitting between side peaks increases whilst the coherent fraction decreases according to Eq. (1).

Frequency-resolved studies of Mollow triplet photon correlations have revealed a rich assortment of physics. An unfiltered Mollow spectrum exhibits antibunching whilst isolating individual peaks results in $g^{(2)}(0) = 1$ for the central Rayleigh peak and antibunching for the side peaks [37–39]. Cross-correlation measurements between the
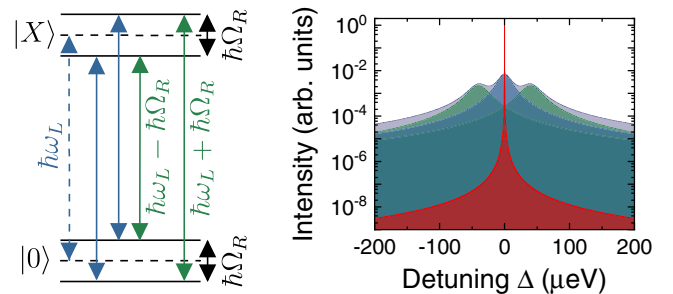
FIG. 3. Theoretical spectrum at $\Omega_R = 2\ \gamma$. Strong driving splits the ground and excited states (dashed) by the Rabi energy ($\hbar\Omega_R$). Two of the four transitions (blue and green) are degenerate (blue), creating a Mollow triplet spectrum (purple) with a narrow coherent component also present (red).

Rayleigh peak and either side peak exhibit antibunching [40] whilst a cross correlation between side peaks exhibits bunching [$g^{(2)}(0) > 1$] [37,38]. In addition, filtering half-way between the central and side peaks has revealed the existence of weak "leapfrog" two-photon transitions that exhibit strong bunching [41,42].

The aforementioned studies were performed with broad filtering ($\Gamma > \gamma$), aside from Ref. [41] where weak bunching [$g^{(2)}(0) \sim 1.2$] was observed when the Rayleigh peak was filtered at $\Gamma \sim 0.25\,\gamma$. Here, the large γ of our sample facilitates thorough exploration of this regime. We begin by measuring $g^{(2)}(0)$ as a function of Ω_R, filtering centered on the Rayleigh peak with $\Gamma = 0.29\,\gamma$. The results [Fig. 4(a)] illustrate a surprising transition from antibunching to strong bunching with increasing Ω_R.

To understand this result requires careful consideration of the relationship between the Rabi frequency Ω_R and the amplitude and filter transmission of the various components of the RF spectrum. The fraction ($\mathcal{F}$) of the filtered ($\Gamma = 0.29\,\gamma$) spectrum arising from each Mollow triplet component is plotted against Ω_R in Fig. 4(b). At small Ω_R, Eq. (1) dictates a large coherent fraction. Thus, the behavior in this region corresponds to Fig. 2(a); only weak antibunching is observed as the filter bandwidth $< \gamma$ removes the majority of the incoherent component. As Ω_R increases, the coherent fraction falls and the splitting of the Mollow triplet increases, reducing the transmission of the side peaks (green) through the filter. It is thus intuitive to expect a

transition to the Poissonian statistics of the Rayleigh peak (blue) [37–39] that now dominates the filtered spectrum.

However, in the limit $\Gamma < \gamma$, the additional effect of "indistinguishability bunching" [18] also becomes relevant. This phenomena originates in the quantum fluctuations of the light field [43,44] and has been observed to lead to photon bunching when filtering at less than the natural linewidth of a light source, even for a classical input state such as a laser [45]. In the case of the RF spectrum considered here, the filtering is narrow compared to the incoherent Rayleigh peak but still broad compared to the coherent component. As such, for larger Ω_R where side peak contributions are negligible, the filtered $g^{(2)}(0)$ of Fig. 4(a) is determined by competition between the Poissonian statistics of the coherent part [see Fig. 2(a)] and bunching originating from the narrowly filtered incoherent part. Therefore, as Ω_R increases, the decreasing coherent fraction allows the indistinguishability bunching effect to dominate, leading to the strong bunching observed for large Ω_R in Fig. 4(a).

Our theoretical model [solid line in Fig. 4(a)] reproduces well the experimental results and predicts a maximum bunching of $g^{(2)}(0) \sim 2.1$ for these parameters. Experimentally, measurements cannot accurately be made at $\Omega_R > 4\gamma$ owing to increasing laser background. We note that theoretical studies [18] predict an ultimate upper limit of $g^{(2)}(0) = 3$ reached at $\Omega_R = 150\gamma$ and $\Gamma = 0.005\gamma$. For solid-state emitters such as the QD studied here, this value
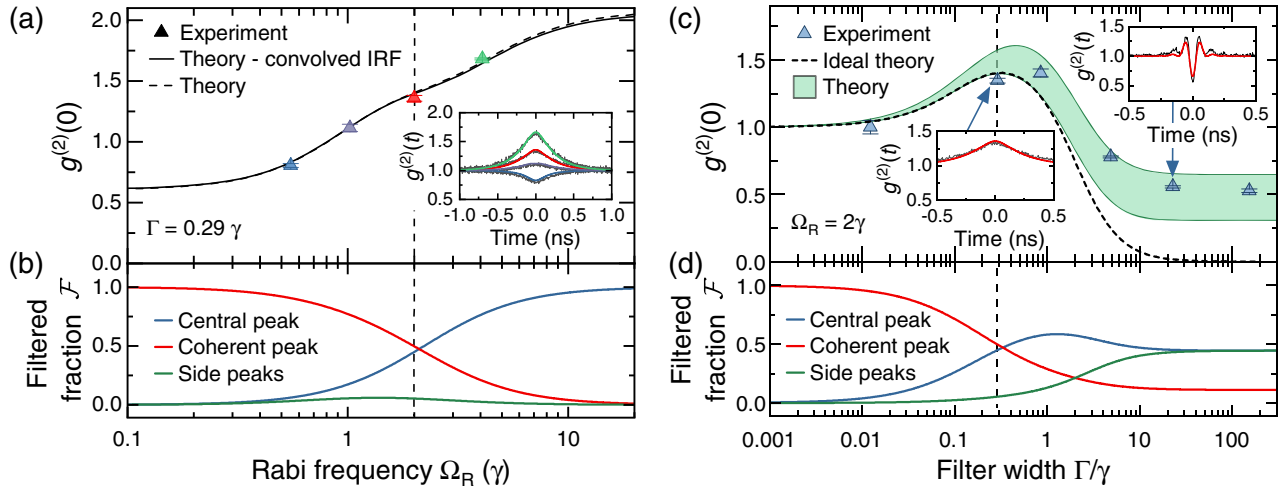
FIG. 4. Filtered photon statistics under strong driving: (a) Measurements (triangles) of $g^{(2)}(0)$ filtered at $\Gamma = 0.29\,\gamma$ transition from antibunching to bunching with increasing Ω_R, lines show the sensor theory prediction with (solid) and without (dashed) detector IRF convolution. Inset: full $g^{(2)}(t)$ measurements from same dataset; lines—model with fitted laser background level. (b) Calculated fraction ($\mathcal{F}$) of the filtered ($\Gamma = 0.29\gamma$) spectrum originating from each Mollow triplet component. (c) Measurements (triangles) of $g^{(2)}(0)$ at $\Omega_R = 2\gamma$ through different filter widths (Γ); dashed line—theory prediction for ideal case, green region—confidence bounds of theory including IRF and laser backgrounds between 0 (lower) and 20% (upper) of the total signal. Insets: full $g^{(2)}(t)$ measurements from the same dataset, Rabi oscillations are observed for $\Gamma > \gamma$. Lines—model with fitted laser background level. (d) Calculated fraction ($\mathcal{F}$) of the filtered spectrum originating from each component. Dashed lines (at $\Omega_R = 2\,\gamma$ and $\Gamma = 0.29\,\gamma$) are equivalent points for comparison between panels (a),(b) and (c),(d).

may not be reached owing to phonon-mediated interactions that cause the coherent fraction to revive at large Ω_R [36].

To further investigate filtering in the strong driving regime, Fig. 4(c) presents a filter width dependence at constant $\Omega_R = 2\,\gamma$. At $\Gamma \gg \gamma$, antibunching is observed in accordance with the expectation for unfiltered RF. The antibunching in this region is degraded due to the period of the Rabi oscillations in $g^{(2)}(t)$ [see Fig. 4(c) inset] being shorter than the detector IRF. Figure 4(d) shows the fraction ($\mathcal{F}$) of the filtered spectrum arising from each component for $\Omega_R = 2\,\gamma$. As Γ becomes comparable to γ in the central region of Fig. 4(c), there is a transition to bunched photon statistics in accordance with Fig. 4(a). This transition originates in the removal of the Mollow side peaks (green) from the filtered spectrum as Γ decreases, combined with the onset of the indistinguishability bunching effect previously described.

As $\Gamma \ll \gamma$ is approached on the left-hand side of Fig. 4(c), $g^{(2)}(0)$ transitions again towards the Poissonian statistics that were observed for $\Gamma \ll \gamma$ in Fig. 2(a). The interpretation here is also the same; for such small Γ the filtered spectrum contains almost solely coherent scattering [red line in Fig. 4(d)] which exhibits Poissonian statistics when spectrally isolated. Ultimately, for very narrow filters of bandwidth comparable to the laser linewidth ($\sim 0.005\gamma$), bunching would be expected to return due to indistinguishability bunching associated with the coherent part of the spectrum. Our theoretical model [green area in Fig. 4(c)] successfully reproduces the experimental behavior, incorporating both the detector IRF and lower and upper bounds corresponding to the measured uncertainty (0–20%) in the laser background contribution to the total signal (see Ref. [19]). It is interesting to note that the upper bound incorporating a 20% background exhibits stronger bunching than the lower bound, indicating the nontrivial effect of introducing an additional Poissonian background.

In summary, we have demonstrated that the resonance fluorescence spectrum of a two-level emitter comprises multiple interfering components that each exhibit distinct photon statistics. Without filtering, these components always interfere to produce the strong antibunching expected from single quantum emitters. However, when spectrally filtering with bandwidth comparable to the natural linewidth (γ) or Rabi frequency (Ω_R), the ratio of these components is modified in the filtered spectrum, leading to strongly modified photon statistics. For weak resonant driving, a suitably narrow filter removes nearly the entire incoherent component, destroying the antibunching and illustrating that a subnatural linewidth and strong antibunching cannot be simultaneously measured. For strong resonant driving, a pronounced bunching effect is observed at filter bandwidths comparable to the natural linewidth before the system ultimately trends towards Poissonian statistics for the narrowest filters. These results illustrate a potential new approach to manipulate the photon statistics of quantum light. In addition, we emphasize that care is required to preserve antibunching when filtering the spectrum of quantum emitters, an important consideration for future high throughput quantum networks where techniques such as wavelength-division multiplexing will be required.

Note added in the proof.—Following the submission of our manuscript we became aware of related results [46].

[*]a.brash@sheffield.ac.uk
[†]ahsan.nazir@manchester.ac.uk

[1] N. Somaschi, V. Giesz, L. De Santis, J. C. Loredo, M. P. Almeida, G. Hornecker, S. L. Portalupi, T. Grange, C. Antón, J. Demory, C. Gómez, I. Sagnes, N. D. Lanzillotti-Kimura, A. Lemaítre, A. Auffeves, A. G. White, L. Lanco, and P. Senellart, Near-optimal single-photon sources in the solid state, Nat. Photonics **10**, 340 (2016).

[2] H. Wang, Z.-C. Duan, Y.-H. Li, S. Chen, J.-P. Li, Y.-M. He, M.-C. Chen, Y. He, X. Ding, C.-Z. Peng, C. Schneider, M. Kamp, S. Höfling, C.-Y. Lu, and J.-W. Pan, Near-Transform-Limited Single Photons from an Efficient Solid-State Quantum Emitter, Phys. Rev. Lett. **116**, 213601 (2016).

[3] F. Liu, A. J. Brash, J. O'Hara, L. M. P. P. Martins, C. L. Phillips, R. J. Coles, B. Royall, E. Clarke, C. Bentham, N. Prtljaga, I. E. Itskevich, L. R. Wilson, M. S. Skolnick, and A. M. Fox, High Purcell factor generation of indistinguishable on-chip single photons, Nat. Nanotechnol. **13**, 835 (2018).

[4] K. De Greve, L. Yu, P. L. McMahon, J. S. Pelc, C. M. Natarajan, N. Y. Kim, E. Abe, S. Maier, C. Schneider, M. Kamp, S. Höfling, R. H. Hadfield, A. Forchel, M. M. Fejer, and Y. Yamamoto, Quantum-dot spin-photon entanglement via frequency downconversion to telecom wavelength, Nature (London) **491**, 421 (2012).

[5] W. B. Gao, P. Fallahi, E. Togan, J. Miguel-Sanchez, and A. Imamoglu, Observation of entanglement between a quantum dot spin and a single photon, Nature (London) **491**, 426 (2012).

[6] A. Delteil, Z. Sun, W.-b. Gao, E. Togan, S. Faelt, and A. Imamoğlu, Generation of heralded entanglement between distant hole spins, Nat. Phys. **12**, 218 (2016).

[7] R. Stockill, M. J. Stanley, L. Huthmacher, E. Clarke, M. Hugues, A. J. Miller, C. Matthiesen, C. Le Gall, and M. Atatüre, Phase-Tuned Entangled State Generation

Between Distant Spin Qubits, Phys. Rev. Lett. **119,** 010503 (2017).

 [8] C. Matthiesen, A. N. Vamivakas, and M. Atatüre, Subnatural Linewidth Single Photons from a Quantum Dot, Phys. Rev. Lett. **108,** 093602 (2012).

 [9] R. Proux, M. Maragkou, E. Baudin, C. Voisin, P. Roussignol, and C. Diederichs, Measuring the Photon Coalescence Time Window in the Continuous-Wave Regime for Resonantly Driven Semiconductor Quantum Dots, Phys. Rev. Lett. **114,** 067401 (2015).

[10] A. J. Bennett, J. P. Lee, D. J. P. Ellis, T. Meany, E. Murray, F. F. Floether, J. P. Griffths, I. Farrer, D. A. Ritchie, and A. J. Shields, Cavity-enhanced coherent light scattering from a quantum dot, Sci. Adv. **2,** e1501256 (2016).

[11] J. Dalibard and S. Reynaud, Correlation signals in resonance fluorescence: Interpretation via photon scattering amplitudes, J. Phys. France **44,** 1337 (1983).

[12] J. C. L. Carreño, E. Z. Casalengua, F. P. Laussy, and E. del Valle, Joint subnatural-linewidth and single-photon emission from resonance fluorescence, Quantum Sci. Technol. **3,** 045001 (2018).

[13] E. Schöll, L. Hanschke, L. Schweickert, K. D. Zeuner, M. Reindl, S. F. Covre da Silva, T. Lettner, R. Trotta, J. J. Finley, K. Müller, A. Rastelli, V. Zwiller, and K. D. Jöns, Resonance fluorescence of GaAs quantum dots with near-unity photon indistinguishability, Nano Lett. **19,** 2404 (2019).

[14] G. Kiršanskė, H. Thyrrestrup, R. S. Daveau, C. L. Dreeßen, T. Pregnolato, L. Midolo, P. Tighineanu, A. Javadi, S. Stobbe, R. Schott, A. Ludwig, A. D. Wieck, S. I. Park, J. D. Song, A. V. Kuhlmann, I. Söllner, M. C. Löbl, R. J. Warburton, and P. Lodahl, Indistinguishable and efficient single photons from a quantum dot in a planar nanobeam waveguide, Phys. Rev. B **96,** 165306 (2017).

[15] L. Dusanowski, S.-H. Kwon, C. Schneider, and S. Höfling, Near-Unity Indistinguishability Single Photon Source for Large-Scale Integrated Quantum Optics, Phys. Rev. Lett. **122,** 173602 (2019).

[16] J. Iles-Smith, D. P. S. McCutcheon, A. Nazir, and J. Mørk, Phonon scattering inhibits simultaneous near-unity efficiency and indistinguishability in semiconductor single-photon sources, Nat. Photonics **11,** 521 (2017).

[17] E. Z. Casalengua, J. C. López Carreño, F. P. Laussy, and E. del Valle, Conventional and unconventional photon statistics, Laser Photonics Rev. **14,** 1900279 (2020).

[18] A. Gonzalez-Tudela, F. P. Laussy, C. Tejedor, M. J. Hartmann, and E. del Valle, Two-photon spectra of quantum emitters, New J. Phys. **15,** 033036 (2013).

[19] See the Supplemental Material at http://link.aps.org/supplemental/10.1103/PhysRevLett.125.043603 for a detailed description of the sensor formalism model used and additional details of the experimental methods employed. This includes Refs. [20–27].

[20] E. del Valle, A. Gonzalez-Tudela, F. P. Laussy, C. Tejedor, and M. J. Hartmann, Theory of Frequency-Filtered and Time-Resolved *n*-Photon Correlations, Phys. Rev. Lett. **109,** 183601 (2012).

[21] E. del Valle, A. Gonzalez-Tudela, F. P. Laussy, C. Tejedor, and M. J. Hartmann, Theory of Frequency-Filtered and Time-Resolved *n*-Photon Correlations, Phys. Rev. Lett.

109, 183601 (2012); Erratum, Phys. Rev. Lett. **116,** 249902 (2016).

[22] A. J. Ramsay, T. M. Godden, S. J. Boyle, E. M. Gauger, A. Nazir, B. W. Lovett, A. M. Fox, and M. S. Skolnick, Phonon-Induced Rabi-Frequency Renormalization of Optically Driven Single InGaAs/GaAs Quantum Dots, Phys. Rev. Lett. **105,** 177402 (2010).

[23] A. Nazir and D. P. S. McCutcheon, Modelling exciton–phonon interactions in optically driven quantum dots, J. Phys. Condens. Matter **28,** 103002 (2016).

[24] H. J. Carmichael, *Statistical Methods in Quantum Optics 1* (Springer-Verlag Berlin Heidelberg, Berlin, 2002), https://doi.org/10.1007/978-3-662-03875-8.

[25] J. Iles-Smith, D. P. S. McCutcheon, J. Mørk, and A. Nazir, Limits to coherent scattering and photon coalescence from solid-state quantum emitters, Phys. Rev. B **95,** 201305(R) (2017).

[26] A. J. Brash, J. Iles-Smith, C. L. Phillips, D. P. S. McCutcheon, J. O'Hara, E. Clarke, B. Royall, L. R. Wilson, J. Mørk, M. S. Skolnick, A. M. Fox, and A. Nazir, Light Scattering from Solid-State Quantum Emitters: Beyond the Atomic Picture, Phys. Rev. Lett. **123,** 167403 (2019).

[27] A. J. Ramsay, A. V. Gopal, E. M. Gauger, A. Nazir, B. W. Lovett, A. M. Fox, and M. S. Skolnick, Damping of Exciton Rabi Rotations by Acoustic Phonons in Optically Excited InGaAs/GaAs Quantum Dots, Phys. Rev. Lett. **104,** 017402 (2010).

[28] C. Cohen-Tannoudji, J. Dupont-Roc, and G. Grynberg, in *Atom—Photon Interactions: Basic Processes and Applications* (Wiley, New York, 1998), pp. 73,369,383, https://doi.org/10.1002/9783527617197.

[29] W. Heitler, *The Quantum Theory of Radiation* (Oxford University Press, Oxford, 1954).

[30] H. S. Nguyen, G. Sallen, C. Voisin, P. Roussignol, C. Diederichs, and G. Cassabois, Ultra-coherent single photon source, Appl. Phys. Lett. **99,** 261904 (2011).

[31] K. Konthasinghe, J. Walker, M. Peiris, C. K. Shih, Y. Yu, M. F. Li, J. F. He, L. J. Wang, H. Q. Ni, Z. C. Niu, and A. Muller, Coherent versus incoherent light scattering from a quantum dot, Phys. Rev. B **85,** 235315 (2012).

[32] F. Y. Wu, R. E. Grove, and S. Ezekiel, Investigation of the Spectrum of Resonance Fluorescence Induced by a Monochromatic Field, Phys. Rev. Lett. **35,** 1426 (1975).

[33] R. H. Brown and R. Q. Twiss, Correlation between photons in two coherent beams of light, Nature (London) **177,** 27 (1956).

[34] Z. X. Koong, D. Scerri, M. Rambach, T. S. Santana, S. I. Park, J. D. Song, E. M. Gauger, and B. D. Gerardot, Fundamental Limits to Coherent Photon Generation with Solid-State Atomlike Transitions, Phys. Rev. Lett. **123,** 167402 (2019).

[35] A. Ulhaq, S. Weiler, C. Roy, S. M. Ulrich, M. Jetter, S. Hughes, and P. Michler, Detuning-dependent Mollow triplet of a coherently-driven single quantum dot, Opt. Express **21,** 4382 (2013).

[36] D. P. S. McCutcheon and A. Nazir, Model of the Optical Emission of a Driven Semiconductor Quantum Dot: Phonon-Enhanced Coherent Scattering and Off-Resonant Sideband Narrowing, Phys. Rev. Lett. **110,** 217401 (2013).

[37] C. A. Schrama, G. Nienhuis, H. A. Dijkerman, C. Steijsiger, and H. G. M. Heideman, Intensity correlations between the components of the resonance fluorescence triplet, Phys. Rev. A **45**, 8045 (1992).

[38] A. Ulhaq, S. Weiler, S. M. Ulrich, R. Roßbach, M. Jetter, and P. Michler, Cascaded single-photon emission from the Mollow triplet sidebands of a quantum dot, Nat. Photonics **6**, 238 (2012).

[39] S. Weiler, D. Stojanovic, S. M. Ulrich, M. Jetter, and P. Michler, Postselected indistinguishable single-photon emission from the Mollow triplet sidebands of a resonantly excited quantum dot, Phys. Rev. B **87**, 241302(R) (2013).

[40] C. A. Schrama, G. Nienhuis, H. A. Dijkerman, C. Steijsiger, and H. G. M. Heideman, Destructive Interference Between Opposite Time Orders of Photon Emission, Phys. Rev. Lett. **67**, 2443 (1991).

[41] M. Peiris, B. Petrak, K. Konthasinghe, Y. Yu, Z. C. Niu, and A. Muller, Two-color photon correlations of the light scattered by a quantum dot, Phys. Rev. B **91**, 195125 (2015).

[42] Y. Nieves and A. Muller, Third-order frequency-resolved photon correlations in resonance fluorescence, Phys. Rev. B **98**, 165432 (2018).

[43] J. A. Armstrong, Theory of interferometric analysis of laser phase noise, J. Opt. Soc. Am. **56**, 1024 (1966).

[44] L. Knöll, W. Vogel, and D.-G. Welsch, Quantum noise in spectral filtering of light, J. Opt. Soc. Am. B **3**, 1315 (1986).

[45] R. C. Neelen, D. M. Boersma, M. P. van Exter, G. Nienhuis, and J. P. Woerdman, Spectral filtering within the Schawlow-Townes linewidth as a diagnostic tool for studying laser phase noise, Opt. Commun. **100**, 289 (1993).

[46] L. Hanschke *et al.*, The origin of antibunching in resonance fluorescence, arXiv:2005.11800.